JACS
JOURNAL OF THE AMERICAN CHEMICAL SOCIETY
Article
pubs.acs.org/JACS

GeSe Thin-Film Solar Cells Fabricated by Self-Regulated Rapid Thermal Sublimation

Ding-Jiang Xue,[†,§,⊥] Shun-Chang Liu,[†,§,⊥] Chen-Min Dai,[‡] Shiyou Chen,[‡] Chao He,[†,§] Lu Zhao,[†,§] Jin-Song Hu,[*,†,§] and Li-Jun Wan[*,†,§]

[†]Beijing National Laboratory for Molecular Sciences, Key Laboratory of Molecular Nanostructure and Nanotechnology, Institute of Chemistry, Chinese Academy of Sciences, Beijing 100190, China

[‡]Key Laboratory of Polar Materials and Devices (MOE), East China Normal University, Shanghai 200241, China

[§]University of Chinese Academy of Sciences, Beijing 100049, China

Supporting Information

ABSTRACT: GeSe has recently emerged as a promising photovoltaic absorber material due to its attractive optical and electrical properties as well as earth-abundant and low-toxic constituent elements. However, no photovoltaic device has been reported based on this material so far, which could be attributed to the inevitable coexistence of phase impurities Ge and $GeSe_2$, leading to detrimental recombination-center defects and seriously degrading the device performance. Here we overcome this issue by introducing a simple and fast (4.8 μm min^{-1}) rapid thermal sublimation (RTS) process designed according to the sublimation feature of the layered structured GeSe. This new method offers a compelling combination of assisting raw material purification to suppress deleterious phase impurities and preventing the formation of detrimental point defects through congruent sublimation of GeSe, thus providing an in situ self-regulated process to fabricate high quality polycrystalline GeSe films. Solar cells fabricated following this process show a power conversion efficiency of 1.48% with good stability. This preliminary efficiency and high stability, combined with the self-regulated RTS process (also extended to the fabrication of other binary IV-VI chalcogenide films, i.e., GeS), demonstrates the great potential of GeSe for thin-film photovoltaic applications.

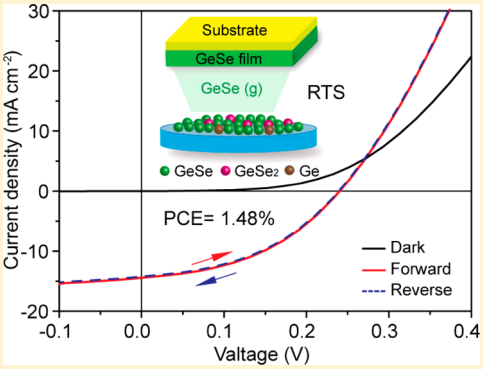

1. INTRODUCTION

Next-generation absorber materials used in thin-film photovoltaics are receiving a growing amount of studies, motivated by the toxicity of Cd and scarcity of In and Te in the current best-developed absorbers, cadmium telluride (CdTe) and copper indium gallium diselenide (CIGS). A promising candidate absorber material should consist of earth-abundant and nontoxic elements, while retaining attractive optical and electrical properties suitable for high-performance photovoltaics. Copper zinc tin sulfoselenide (CZTSSe) is one of the most intensively studied materials in this field, currently demonstrating a record power conversion efficiency (PCE) of 12.6%.[1] However, theoretical and experimental studies have revealed several important issues with CZTSSe, most of which originate from Cu−Zn and Sn−Zn antisite disorder and narrow phase stability range of this multicomponent material.[2−6] This situation therefore brings renewed attention to the study of simpler binary earth-abundant and environmentally friendly compounds such as Sb_2Se_3 and SnS, both of which have recently shown substantial progress within a very short time, achieving impressive certified PCEs of 5.6% and 4.36%,[7,8] respectively.

In this aspect, germanium monoselenide (GeSe), a simple binary IV-VI chalcogenide, also fulfills these criteria and thus is a very promising candidate as a photovoltaic absorber material for several key reasons: (1) Its constituent elements of Ge and Se are relatively earth-abundant and low-toxic in nature.[9,10] This feature gives it an advantage over conventional CdTe and CIGS where toxic or rare elements are required. (2) GeSe exhibits attractive optical properties for photovoltaic application. It has closely placed indirect and direct band gaps in the range of 1.1−1.2 eV,[11,12] overlapping fairly well with the solar spectrum for a single junction solar cell and thus enabling a Shockley−Queisser efficiency limit of ∼30%;[13] it shows a high absorption coefficient (>10^4 cm^{-1}) at wavelength close to the absorption onset,[14,15] permitting absorbing most of the solar energy above the band gap within one micrometer thick layer. Theoretical calculations revealed that the lower part of conduction band is mainly composed of Ge 4p orbitals due to the existence of the lone-pair $4s^2$ electrons present on bivalent Ge, whereas the filled Se valence 4p orbitals primarily form the higher part of valence band, thus leading to the $p-p$

Received: November 11, 2016
Published: December 20, 2016

DOI: 10.1021/jacs.6b11705
J. Am. Chem. Soc. 2017, 139, 958−965

optical transition with high joint density of states and hence a strong absorption coefficient.[14] (3) GeSe is intrinsically *p*-type with hole mobility up to 128 $cm^2 V^{-1} s^{-1}$, even higher than that of CdTe, thereby enabling efficient photogenerated carrier transport and collection.[16] (4) GeSe adopts an orthorhombic crystal structure with *Pnma* 62 space group at room temperature.[17,18] It consists of double-layer slabs of 3-fold covalently coordinated Ge−Se in a chair configuration separated from one another by weak van der Waals forces,[19] as shown in Figure 1. Similar to Sb_2Se_3 with one-dimensional

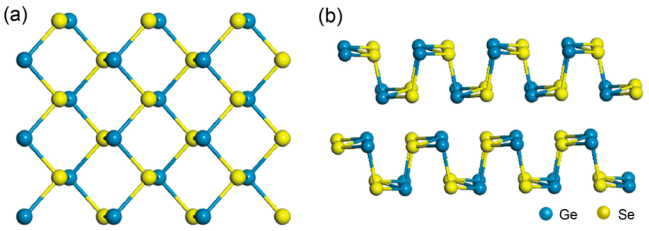

Figure 1. Crystal structure of orthorhombic GeSe from (a) top and (b) side view.

crystal structure,[7] this type of two-dimensional layered crystal structure with limited dangling bonds is expected to provide a chemically inert surface with low surface defect density, leading to a high chemical and environmental stability while partly minimizing the carrier recombination loss at grain boundaries (GBs).[20,21] (5) GeSe has impressively high vapor pressures at temperatures below its melting point of 670 °C,[22,23] much higher than that of CdTe, as shown in Figure S1 (Supporting Information). This feature makes GeSe ideal for thermal sublimation deposition for growing high quality films, a high-throughput and low-cost deposition technique that has been successfully applied in industrial manufacturing of CdTe solar cells;[24,25] more importantly, the GeSe raw material may be purified by the process of sublimation during the film growth while leaving possible deleterious impurities in source, endowing a novel in situ self-purification. The low-cost and efficient deposition technique, together with the demand of low purity of raw material, would remarkably reduce the module manufacturing cost, despite the relatively high price of Ge, which may be reduced in the future due to the high earth-abundance of Ge.[26] All the aforementioned features make GeSe worth exploring for photovoltaic application.

Until now, however, no photovoltaic device has yet been reported based on this material. The main reason may lie in the lack of simple and benign methods for the fabrication of high quality polycrystalline GeSe thin film, which usually suffers from the inevitable coexistence of phase impurities Ge and $GeSe_2$ as evidenced by the Ge−Se binary phase diagram,[23] thereby delaying its further photovoltaic application. To date, there are only limited reports focusing on the characterization of amorphous GeSe film produced by sputtering or thermal evaporation,[27,28] which cannot be directly used as photovoltaic absorber layer due to its high defect states. In addition, although there are also several studies devoted to the synthesis of GeSe nanostructures including nanosheets and nanobelts and their further application in photodetectors,[17,18] many photovoltaic-relevant properties of GeSe, such as the conduction band and valence band position, remain unclear at present; meanwhile, processing GeSe into nanostructures might not be necessary for photovoltaic application due to the large amount of GBs, significantly degrading the device performance via recombination losses. Consequently, it is highly desirable to develop a simple and reliable approach to fabricate high quality polycrystalline GeSe thin film and fully evaluate its potential for solar cell application.

Here, we propose a rapid thermal sublimation (RTS) strategy to fabricate device-quality GeSe thin films, designed according to the newly developed rapid thermal evaporation (RTE), a technique Tang et al. first introduced to produce Sb_2Se_3 thin-film solar cells.[7] This developed film deposition technique utilizes low-cost rapid thermal processing (RTP) system, requires low-vacuum (~1 Pa) maintained only by a mechanical pump, offers a novel in situ self-regulated process employing raw GeSe powders as purchased without any further purification, and enables fast deposition rate (up to 4.8 $\mu m\ min^{-1}$), thus making it highly appealing for the growth of GeSe film. Guided by the detailed theoretical and experimental investigation of the sublimation mechanism of GeSe, we then carefully optimized the film deposition procedure, obtained high quality GeSe film through RTS, and systematically studied the material, optical, and electrical properties of as-prepared films, and finally built a superstrate ITO/CdS/GeSe/Au solar cell with 1.48% efficiency, fully indicating that GeSe is indeed a very promising absorber material for thin-film solar cells.

2. EXPERIMENTAL SECTION

2.1. Chemicals. Germanium monoselenide (GeSe, powder, 99%) was purchased from Jiangxi Ketai Advanced Materials Co. Ltd. Thiourea (CH_4N_2S, 99%) and anhydrous cadmium sulfate ($CdSO_4$, 99%) were purchased from Alfa Aesar. Ammonia solution ($NH_3{\cdot}H_2O$, analytical reagent grade) was purchased from Beijing Chemical Factory. All chemicals were used as received without any further purification.

2.2. GeSe Film Deposition. GeSe films were fabricated by RTS in a tube furnace (MIT, Hefei, China). GeSe powder was uniformly placed onto the washed soda lime glass and then the glass was loaded on top of the AlN plate inside the quartz boat, and the ITO substrate was suspended onto the quartz boat (0.8 cm above GeSe powder) with the ITO side facing down. Vacuum was maintained at 1 Pa through a simple mechanical pump, and the temperature was controlled through the infrared heaters surrounding the quartz tube and monitored by the thermal couple. The deposition process was to first preheat the source and substrate at 350 °C for 20 min, then quickly increased the source temperature up to 400 °C within 2 s, maintained this temperature for 5 s, and finally turned off the heating while introducing N_2 into the tube furnace and allowed the film to cool down naturally. Note that a graphite lid was covered on top of the substrate, which was used to stabilize the substrate temperature during the rapid sublimation process of 7 s due to the large heat capacity of the glass substrate and the graphite lid. The corresponding temperature profile during the RTS process was shown in Figure S2.

2.3. Solar Cell Fabrication. GeSe thin-film solar cells were fabricated with a conventional superstrate structure of glass/ITO/CdS/GeSe/Au. First, CdS buffer layer was deposited on ITO glass by chemical bath deposition (CBD) according to a previously reported procedure.[29] Then, GeSe layers were deposited by RTS described above. Finally, Au back contacts were deposited by thermal evaporation through a shadow mask on the top of devices. Each device had an active area of 0.09 cm^2 fixed by the mask pattern.

2.4. Materials and Device Characterization. TGA (PerkinElmer Instruments, Diamond TG/DTA6300) was performed in a flowing N_2 atmosphere at 10 °C/min to study the weight loss of GeSe powder at elevated temperatures. MS spectra were acquired on a GCT-MS instrument (Waters, Manchester, UK). Powder X-ray diffraction (XRD) patterns were recorded on a Regaku D/Max-2500 diffractometer equipped with a Cu $K\alpha_1$ radiation (λ = 1.540 56 Å). Raman spectrum (Horiba JobinYvon, LabRAM HR800) was measured under the excitation line of 532 nm. X-ray photoelectron spectroscopy (XPS)

DOI: 10.1021/jacs.6b11705
J. Am. Chem. Soc. 2017, 139, 958−965

measurements were performed on an ESCALab220i-XL electron spectrometer (VG Scientific) using 300W Al Kα radiation. The composition of the films was determined by electron probe microanalysis (EPMA-1720, SHIMADZU). The optical transmittance of GeSe film was recorded by UV−vis-near IR spectrophotometer (UH4150, HITACHI). Ultraviolet photoemission spectroscopy (UPS, Specs UVLS, He I excitation, 21.2 eV, referenced to the Femi edge of argon etched gold) was employed to detect the Fermi level and valence band of GeSe film. Electrical properties of GeSe films were determined by Hall measurement (Ecopia HMS-5500, with gold electrode). Scanning electron microscopy (SEM) images were obtained by Hitachi S-4800 microscrope. Atomic force microscopy (AFM) data was collected on a Bruker Dimension Icon microscope. Device performance was measured with a solar simulator (Newport, USA) equipped with 450 W xenon lamp (OSRAM) and a Keithley 2420 source meter. Light intensity was adjusted using a NREL-certified Si solar cell with a KG^{-2} filter for approximating AM 1.5G light (100 mW cm^{-2}). EQE of solar cells was measured with a lock-in amplifier. For the EQE measurement, light source was generated by a 300 W xenon lamp of Newport (Oriel, 69911, Newport Corporation, Irvine, CA, USA) and then was split into specific wavelength using Newport Oriel cornerstone 130 1/8 monochromator (Oriel, model 74004, Newport Corporation, Irvine, CA, USA).

2.5. Calculation Method. The crystal structure, total energy and band structure were calculated using the density functional theory (DFT) methods as implemented in the Vienna ab initio simulation package (VASP) code.[30] The frozen-core projector augmented-wave (PAW) pseudopotentials and plane wave basis set with an energy cutoff of 520 eV were employed, with a 8 × 8 × 4 Monkhorst−Pack k-point mesh included in the Brillouin zone integration for the 16-atom primitive cell and a 3 × 3 × 3 mesh for the 64-atom supercell.[3,20]

3. RESULTS AND DISCUSSION

3.1. Experimental and Theoretical Investigation of the Sublimation Mechanism of GeSe. To guide the rational design for RTS process, we first investigated the sublimation mechanism of GeSe. Mass spectrometry (MS) was introduced as a powerful characterization method to explore the sublimation mechanism of GeSe, which can directly monitor the sublimation process,[31] thus explaining detailed mechanism through interception of the vapor phase over solid GeSe for structural characterization. As shown in Figure 2a,b, under the test condition of heating temperature at 400 °C, it was obvious

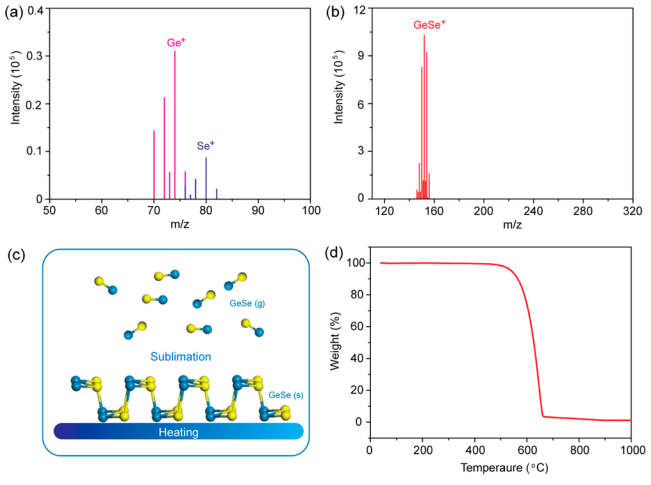

Figure 2. (a, b) Mass spectra of vapor species above GeSe (s) at the temperature of 400 °C. (c) Schematic of the sublimation mechanism of GeSe. (d) TGA of GeSe powder in a N_2 flowing environment at 10 °C min^{-1} ramp rate.

that the dominant components of the vapor phase sublimed from GeSe (s) were the diatomic molecules GeSe (g) with the identical stoichiometry as the solid phase, while detecting minor species of Ge (g) and Se (g), approximately only 1% intensity of GeSe (g). The accompanying peaks in Figure 2a,b should be ascribed to the isotopes of Ge and Se. Combined with no signal of higher molecular weight species, we proposed that the sublimation of GeSe may be processed by forming the most abundant products of GeSe (g) through the following reaction: GeSe (s) = GeSe (g) (Figure 2c), in good agreement with the sublimation mode of IV-VI monochalcogenides, and rather than II-VI compounds which generally sublimed under practically complete decomposition into elemental species.[22,32] This stoichiometric sublimation style could possess the natural advantage to suppress effectively the formation of detrimental point defects such as deep-level vacancies, interstitials and antisites, greatly superior to decomposing sublimation, which predictably gave rise to harmful point defects due to the quite different vapor pressures of decomposition products.

To understand thoroughly why GeSe can sublime easily via the diatomic molecule, we calculated the energy difference of GeSe between the diatomic-molecule gas phase (GeSe molecule gas) and the solid phase (crystal). The energy difference is only 1.40 eV/2-atom, meaning that it costs only 1.40 eV for GeSe to transform from the solid state to the GeSe gas state. In contrast, the energy difference of GeSe between the single-atom gas phase (separated Ge and Se atomic gas) and the solid phase (crystal) is much higher (8.44 eV/2-atom) than that (1.40 eV/2-atom) between the diatomic-molecule gas phase and the solid phase. That means the sublimation to the separated Ge and Se atomic gas costs much higher energy than to the diatomic GeSe molecule gas, explaining why only diatomic molecule GeSe (g) was detected in the MS whereas only minor species of Ge (g) and Se (g) were detected.

We also calculated the energy difference for the zincblende structured photovoltaic semiconductors such as CdTe, which is much larger (3.24 eV/2-atom for the sublimation to diatomic-molecule CdTe gas phase and 2.59 eV/2-atom for the sublimation to the separated Cd and Te_2 gas). This explains why GeSe can sublime more easily than CdTe, and why GeSe sublimes via the diatomic-molecule gas while CdTe through the elemental gas.

Considering the layered structure of GeSe, we think that its small energy difference between the diatomic-molecule gas and solid phases should result from the less coordination number of Ge and Se in the GeSe structure, i.e., each Ge (Se) is bonded only with 3 Se (Ge) atoms, as shown in Figure 1. In the zincblende-structured CdTe, the coordination number is 4, so it breaks more bonds when they transform from the solid state to the gas state. According to this analysis, the energy difference of GeS, which also has a layered structure, should be low too. The calculated results in Table 1 supported this analysis. Therefore, we predict that the RTS process designed for GeSe may also be used for the fabrication of GeS thin film, and the preliminary results are shown in Figure S3.

3.2. Guidelines of RTS Process. With regard to sublimation, an important endothermic phase transition, sublimation temperature and corresponding vapor pressure are the key and fundamental parameters for the RTS process; therefore, temperature-dependent vapor pressure of GeSe was first calculated according to the following equation: $\log p = A - B/T$, where A is 8.51, B is 8824, T is the absolute temperature in K, and p is the vapor pressure in atmosphere (atm).[22] As

DOI: 10.1021/jacs.6b11705
J. Am. Chem. Soc. 2017, 139, 958−965

Table 1. Calculated Total Energy (in eV/2-atom) of XY (GeSe, GeS, and CdTe) in the Crystal Solid Phase XY (s), Diatomic-Molecule Gas Phase XY (g) and Single-Atom Gas Phase X (g) + Y (g), and Their Energy Difference[a]

XY	XY (s)	XY (g)	XY (g) − XY (s)	X (g) + Y (g)	X (g) + Y (g) − XY (s)
GeSe	−8.47	−7.07	1.40	−0.03	8.44
GeS	−9.16	−7.80	1.36	−0.03	9.13
CdTe	−4.81	−1.57	3.24	−2.22	2.59

[a]Note that the Y (g) for CdTe represents Te_2 (g) rather than Te (g).

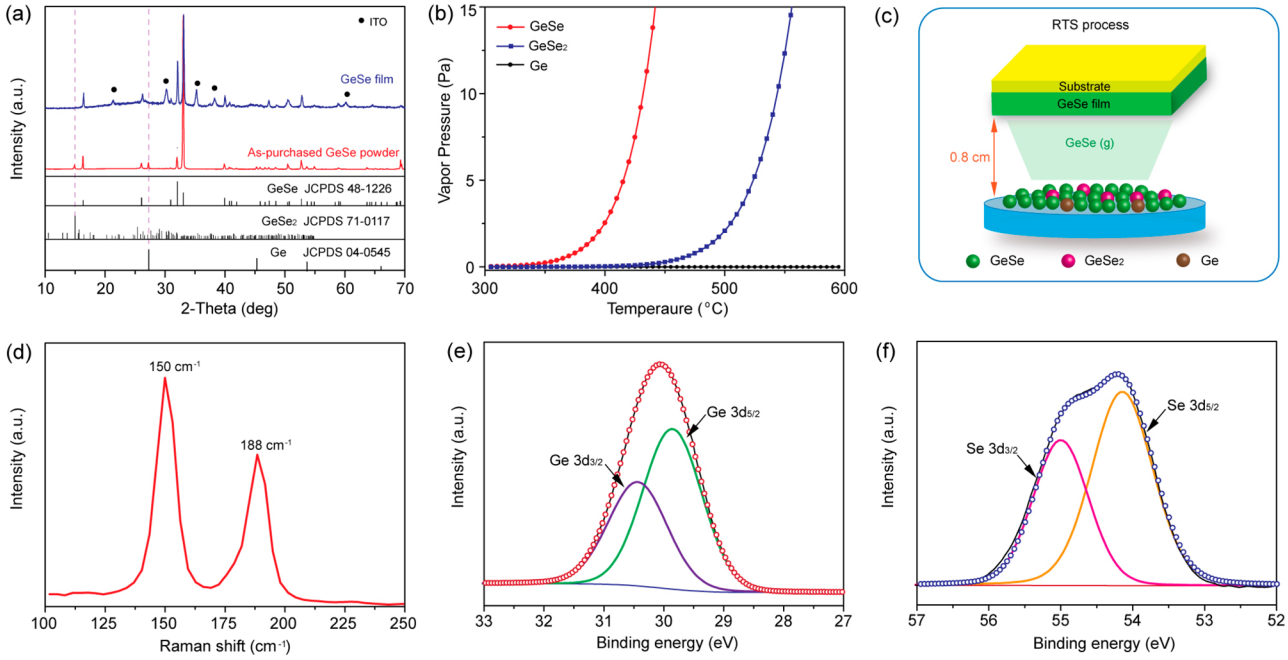

Figure 3. (a) XRD patterns of as-purchased GeSe powder and GeSe thin film deposited on ITO substrate. (b) Temperature-dependent vapor pressure of GeSe, $GeSe_2$, and Ge in the temperature range from 300 to 600 °C. (c) Schematic diagram of RTS process for GeSe film deposition. (d) Raman spectrum of GeSe film. XPS spectra of (c) Ge 3d and (d) Se 3d in GeSe thin film.

shown in Figure 3b (red curve), it is clear that GeSe has very high vapor pressure at elevated temperatures even below its melting point (670 °C), 2.54 Pa at 400 °C and 126.02 Pa at 500 °C, indicating its feature of easy sublimation.

Moreover, thermogravimetric analysis (TGA) of GeSe powder was employed to guide further the optimization of RTS. Figure 2d shows that weight loss of GeSe started at approximately 470 °C, and sharply completed before its melting point, consistent with the above calculated results. Clearly, during the RTS process, rapid sublimation would occur when GeSe power is heated up nearby 470 °C or even below this temperature due to the higher vacuum in RTS (~1 Pa) compared with that of TGA measurement (typically 1 atm). Guided by the above information, we can come to the conclusion that the substrate temperature during RTS process should not exceed 470 °C; otherwise, GeSe already deposited on the substrate would resublime, thus reducing the deposition efficiency. Finally, we chose 400 °C as the source sublimation temperature due to the proper vapor pressure (2.54 Pa) at this temperature, a suitable pressure achieving a balance between fast sublimation and high quality GeSe films.[33] The RTS fabrication details were described in the Experimental Section.

3.3. Fabrication and Material Characterization of GeSe Film. Phase impurities in absorber material usually act as recombination centers, leading to severe carrier recombination loss and thus low device efficiency. Therefore, purification of those impurities is mandatory for all kinds of solar cells to achieve high efficiency. We first applied X-ray diffraction (XRD) to study carefully the possible phase impurities in GeSe raw materials. As shown in Figure 3a (red curve), there was a certain amount of phase impurities $GeSe_2$ and Ge present in as-purchased GeSe powder. The XRD result indicated that although the purchased GeSe powder was prepared nominally 99% pure Ge and Se, the GeSe and phase impurities $GeSe_2$ and Ge were not distinguishable. This observation could be explained by the Ge−Se binary phase diagram where slight GeSe may be oxidized by element Se to form $GeSe_2$ while leaving the unreacted element Ge,[23] when GeSe was prepared by mixing the elements Ge and Se with Ge/Se molar ratio of 1:1. Note that those phase impurities may inevitably remain in the final GeSe film fabricated by the conventional deposition methods (i.e., sputtering). Fortunately, vapor pressures of $GeSe_2$ (0.027 Pa, 400 °C) and Ge (1.105×10^{-16} Pa, 400 °C) were substantially lower than that of GeSe (2.54 Pa, 400 °C), as shown in Figure 3b and Table S1. This feature enabled the desired GeSe to deposit onto the substrate while leaving the phase impurities of $GeSe_2$ and Ge in the source simply through the control of source temperature during our RTS process, as schematically illustrated in Figure 3c. This strategy actually offered an in situ self-purified process, enabling a direct utilization of low-purity raw materials to achieve device-quality solar absorber films, and hence greatly reducing the cost of raw materials.

DOI: 10.1021/jacs.6b11705
J. Am. Chem. Soc. 2017, 139, 958−965

On the basis of the above vapor pressure analysis, we successfully obtained phase-pure GeSe films through RTS. As shown in Figure 3a (blue curve), all of the diffraction peaks matched well with orthorhombic GeSe (JCPDS 48-1226) without any phase impurities ($GeSe_2$ or Ge). The refined orthorhombic lattice parameters calculated from the experimental diffraction pattern were a = 10.839 Å, b = 3.839 Å, and c = 4.378 Å, agreeing well with the JCPDS database (a = 10.840 Å, b = 3.834 Å, and c = 4.390 Å). It was noteworthy that the diffraction intensity associated with the (400) peak was much stronger than that for the (111) peak, indicating the as-prepared GeSe film could be oriented along [100] and horizontally stacked in parallel with the substrate. Moreover, the Raman spectrum of GeSe film showed two distinct peaks centered at 150 and 188 cm^{-1} (Figure 3d), corresponding to the typical B_{2u} and A_g vibrational modes of GeSe respectively, whereas no evidence of other possible phases appeared in the Raman spectrum.[34] X-ray photoelectron spectroscopy (XPS) measurement was further carried out on the as-prepared GeSe film to detect whether there were any Ge^{4+} or element Ge components. As shown in Figure 3e, magnified XPS spectrum of Ge showed a 3d doublet with an excellent fitting at the binding energy of 29.85 eV ($3d_{5/2}$) and 30.43 eV ($3d_{3/2}$) with a separation of 0.58 eV, in good agreement with the expected binding energy in GeSe.[35] The perfect Gaussian−Lorentzian peak fitting confirmed the absence of Ge^{4+} and Ge^0 in the sample within XPS detection limit. Analogously, magnified XPS spectrum of Se (Figure 3f) revealed that Se was in the expected valence state of $Ge^{2+}Se^{2-}$, confirming the film prepared by RTS was phase-pure GeSe. In addition, the composition of as-prepared GeSe film was determined by electron probe microanalysis (EPMA), which corresponded well with the stoichiometry of GeSe, as shown in Figure S4. In brief, the above material characterizations performed by XRD, Raman, XPS, and EPMA showed that the obtained GeSe films deposited by RTS process were phase-pure GeSe without any phase impurities $GeSe_2$ or Ge originally present in raw materials. Overall, the in situ self-purification enabling the direct use of low-cost raw materials, combined with the congruent sublimation style of GeSe preventing the formation of detrimental point defects, endows our RTS process with a novel self-regulated feature to fabricate high quality polycrystalline GeSe films.

3.4. Optical and Electrical Characterization of GeSe Film. Optical properties of GeSe film were characterized by transmission spectroscopy. As shown in Figure 4a, transmittance began to sharply decline at the wavelength of approximately 1100 nm, and gradually decreased to almost zero at wavelength shorter than 900 nm. The wave dependent absorption coefficient of GeSe film was further calculated based on the following simplified formula: $\alpha = d^{-1}\ln(T^{-1})$, where d is the thickness of GeSe film directly measured from cross-sectional scanning electron microscopy (SEM) and T is the transmittance. Figure 4b shows that the absorption coefficient of GeSe film remained over 10^4 cm^{-1} for approximately 1.2 eV photons, in agreement with theoretically calculated value and comparable to that of CIGS and CZTS absorbers.[36,37] It should also be noted that the slow increase in absorption coefficient between 1.1 and 1.2 eV might be attributed to the indirect optical transition nature of GeSe in this range, whereas there was a sharp increase above 1.2 eV due to the direct transition.[38,39] Furthermore, as shown in Figure 4b inset, by plotting $(\alpha h\nu)^{1/2}$ versus $(h\nu)$ we extrapolated the linear fitting

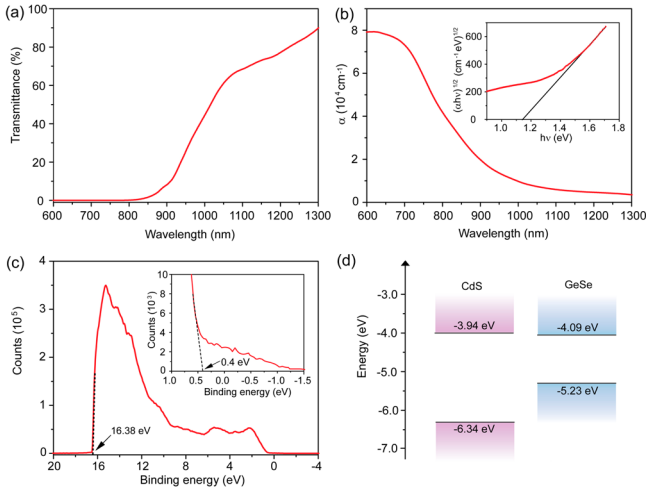

Figure 4. (a) Transmittance spectrum of GeSe film on ITO substrate. (b) Wavelength-dependent absorption coefficient of GeSe film. Inset: Tauc plot (n = 1/2, indirect) for GeSe film. (c) UPS spectrum of GeSe film. Inset plot is the fitting of the long-tail spectrum. (d) Energy band diagram of CdS and GeSe film calculated from the Tauc plot and UPS results.

line with the x-axis and obtained a band gap of 1.14 eV, matching well with previously reported results for GeSe.[11,12]

Ultraviolet photoelectron spectroscopy (UPS) was used to determine the valence band maximum (VBM) and Fermi energy of our GeSe films. As shown in Figure 4c, Fermi energy was first obtained as −4.83 eV by subtracting the spectrum onset of 16.38 eV with the ultraviolet photoelectron energy of 21.21 eV. By linear extrapolation in low binding energy region, the distance between Fermi energy and VBM was calculated as 0.4 eV (Figure 4c, inset). Using the measured band gap of 1.14 eV from the transmission spectrum, we thus calculated the VBM and conduction band minimum (CBM) of our GeSe film at −5.23 and −4.09 eV, respectively (Figure 4d). Moreover, the position of the Fermi energy closer to the VBM indicated the p-type conductivity of as-prepared GeSe film.

Electrical properties of GeSe films were investigated by Hall measurement at 300 K. Au was selected as electrodes and deposited onto GeSe films to form ohmic contact, as evidenced by the linear current−voltage (I−V) curve shown in Figure S5. The positive Hall coefficient revealed that as-prepared GeSe film was p-type conductivity, consistent with the conclusion from our UPS measurement and previous reports.[18] Meanwhile, the resistivity, majority carrier (hole) mobility and concentration tested using Van Der Pauw method were estimated to be 2.18 × 10^2 Ω cm, 14.85 cm^2 V^{-1} s^{-1}, and 1.93 × 10^{15} cm^{-3}, respectively. Compared with the reported high hole mobility of 128.7 cm^2 V^{-1} s^{-1} measured from GeSe single crystal,[16] the low mobility of our GeSe film could be attributed to the extra GBs scattering in polycrystalline films, thus indicating that there was also much room left for further improvement through promoting crystalline grain growth. It should be noted that this mobility was still very encouraging and higher than that of many other photovoltaic materials with high device performance such as Sb_2Se_3 (5.1 cm^2 V^{-1} s^{-1}) and SnS (10 cm^2 V^{-1} s^{-1}).[40,41] The measured low hole concentration may arise from the very slight deviation from stoichiometry and the high purity of our GeSe films prepared by our self-regulated RTS process. This low hole concentration could enable the depletion region, covered by built-in field, to

DOI: 10.1021/jacs.6b11705
J. Am. Chem. Soc. 2017, 139, 958−965

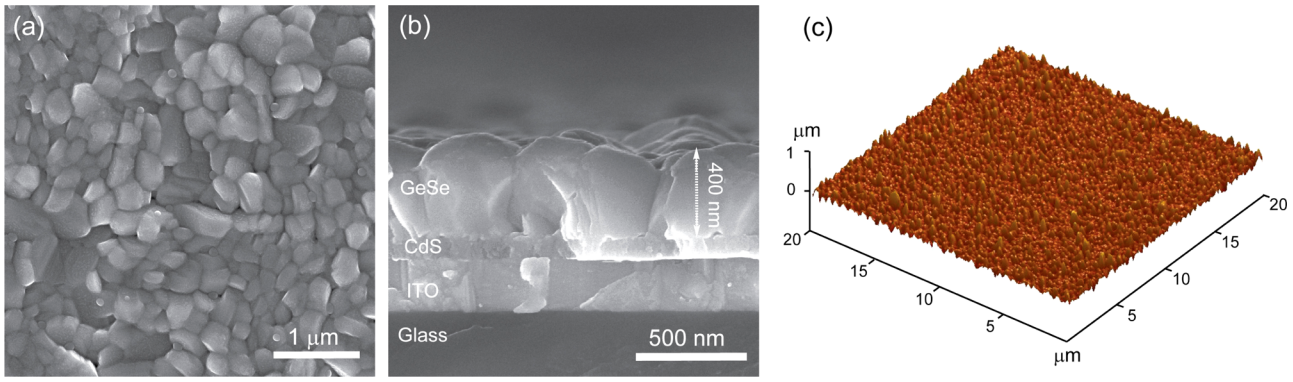

Figure 5. (a) Top-view and (b) cross-sectional SEM images of GeSe film deposited on top of CdS layer. (c) AFM image of GeSe film.

extend through most of the GeSe absorber layer, thus facilitating the charge transport and collection in solar cells.

3.5. GeSe Thin-Film Solar Cell Fabrication and Performance. Finally, we estimated the potential of our GeSe thin films as photovoltaic absorber by fabricating superstrate ITO/CdS/GeSe/Au solar cells, as shown in Figure 6a. CdS was chosen as the buffer layer due to the optimal band offset with GeSe, facilitating photogenerated electrons flowing from GeSe to CdS.[42] Our GeSe film was then deposited onto the CdS layer through the optimized RTS process. As shown in Figure 5a, as-obtained GeSe film was of high quality with well crystallized grains close to 300 nm and free of cracks and pinholes, an evidence of the feasibility to use RTS method to deposit GeSe films. For transmission electron microscopy (TEM) characterization, the sample was prepared by cross-sectioning the as-prepared GeSe film using a focused ion beam (FIB). The cross-sectional TEM images showed that the GeSe film was compact and well-crystallized with clear lattice fringes corresponding (400) planes of orthorhombic GeSe (Figure S6a,b). We applied scanning transmission electron microscopy-energy dispersive X-ray spectroscopy (STEM-EDS) elemental mapping to identify the element distribution of the GeSe film. The element maps of Ge and Se showed that the distributions of two elements were highly homogeneous within the film (Figure S6d). Atomic force microscopy (AFM) analysis further showed that as-prepared GeSe film was smooth with a surface roughness of 63.1 nm (Figure 5c and Figure S7). In addition, the film thickness was directly measured to be around 400 nm from Figure 5b, sufficient to absorb much of incident sunlight due to the large absorption coefficient of GeSe, while clearly demonstrating that the deposition rate of our RTS process was as high as 4.8 μm min^{-1}, much faster than that of other traditional deposition strategies such as thermal evaporation (typically 0.01−0.1 μm min^{-1}) and sputtering (typically 0.01−0.05 μm min^{-1}).[7] Upon Au electrodes deposition, the device was finished.

Under 100 mW cm^{-2} simulated AM 1.5G irradiation, our champion solar cell exhibited an efficiency of 1.48%, with a short-circuit current density (Jsc) of 14.48 mA cm^{-2}, open-circuit voltage (Voc) of 0.24 V, and fill factor (FF) of 42.60% (Figure 6b), the first observed photovoltaic effect in the GeSe based device. In strong contrast to organic−inorganic hybrid perovskite solar cells, no hysteresis between forward (Jsc to Voc) and reverse (Voc to Jsc) scans was observed in our device. This hysteresis-free behavior might be attributed to the strong covalent character of GeSe arising from the little difference in electronegativity between Ge (2.01) and Se (2.55),[43] compared

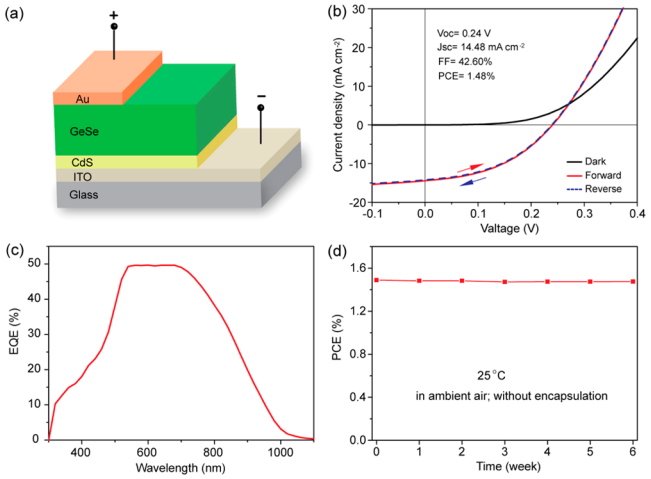

Figure 6. (a) Schematic configuration of CdS/GeSe superstrate solar cell. (b) Forward and reversed $J-V$ curves of GeSe solar cell performance in the dark and under 100 mW cm^{-2} simulated AM1.5G irradiation, respectively. (c) EQE spectrum of GeSe solar cell. (d) Stability of a typical device without encapsulation stored under regular laboratory conditions (ambient air, no shading).

with the highly ionic bonding in perovskite halides causing the ion migration.[44,45] The corresponding external quantum efficiency (EQE) was presented in Figure 6c. The EQE spectrum peaked at 540−700 nm, whereas declined at shorter and longer wavelength, due to the strong absorption of CdS buffer layer and insufficient generation and collection of carriers far from the heterojunction, respectively. Compared with the above 90% plateau of EQE spectrum observed in highly efficient CZTSSe solar cells, this low EQE value could possibly suffer from the interfacial defects and the GeSe film orientation. Despite the high quality of GeSe films deposited by RTS process, our GeSe solar cell suffered from a low device efficiency. The main reason could be the poor GeSe/CdS heterojunction as evidenced by the low rectification of $J-V$ curve in the dark shown in Figure 6b. The device performance could be further boosted by passivating interfacial defects, substituting CdS with other buffer layer such as ZnO and TiO_2, optimizing device configuration, and adding an antireflection coating, since the Shockley−Queisser efficiency limit for GeSe with a band gap of 1.14 eV is about 30%.

We further investigated the device stability of our GeSe solar cells. As shown in Figure 6d, the PCE of our best device without any encapsulation experienced no obvious degradation after 6 weeks ambient storage in a typical laboratory

DOI: 10.1021/jacs.6b11705
J. Am. Chem. Soc. 2017, 139, 958−965

environment, outperforming many next generation solar cells such as organic−inorganic hybrid perovskite and polymer solar cells when no encapsulation was applied. This good device stability might mainly depend on the high degree of air stability of GeSe absorber layer, as evidenced in Figure S8. In sum, the preliminary device performance and stability are very encouraging considering the simple self-regulated RTS process as well as the very limited optimization work done so far, and ongoing work is focused on further improving device performance.

4. CONCLUSIONS

In conclusion, we have introduced a simple in situ self-regulated RTS process to fabricate high quality polycrystalline GeSe thin films. The as-deposited film had a suitable band gap of 1.14 eV with high absorption coefficient ($>10^4$ cm^{-1}), and showed *p*-type conductivity with hole mobility of 14.85 cm^2 V^{-1} s^{-1}. Superstrate CdS/GeSe thin-film solar cells were constructed and exhibited a PCE of 1.48% with good stability. Overall, earth-abundant and low-toxic constituent elements, attractive optical and electrical properties, as well as the simple self-regulated RTS process, confirms the great potential of GeSe for thin-film solar cell applications.

■ ASSOCIATED CONTENT

Supporting Information

The Supporting Information is available free of charge on the ACS Publications website at DOI: 10.1021/jacs.6b11705.

Temperature-dependent vapor pressure of GeSe and CdTe, temperature profile of the RTS process, XRD patterns of as-purchased GeS powder and GeS film, EPMA spectrum of GeSe thin film, *I*−*V* characteristic between two Au electrodes on GeSe thin film, cross-sectional TEM image of the GeSe device, and XRD patterns, photographs, AFM and SEM images of GeSe film (PDF)

■ AUTHOR INFORMATION

Corresponding Authors

*hujs@iccas.ac.cn

*wanlijun@iccas.ac.cn

ORCID

Li-Jun Wan: 0000-0002-6268-0959

Author Contributions

⊥These authors contributed equally.

Notes

The authors declare no competing financial interest.

■ ACKNOWLEDGMENTS

This work is supported by the National Key Project on Basic Research (2015CB932302), the National Natural Science Foundation of China (21573249, 21403078), the Strategic Priority Research Program of the Chinese Academy of Sciences (Grant No. XDB12020100) and the Youth Innovation Promotion Association CAS. We thank Prof. H. L. Dong and Z. X. Nie at ICCAS for their helpful discussion.

■ REFERENCES

(1) Wang, W.; Winkler, M. T.; Gunawan, O.; Gokmen, T.; Todorov, T. K.; Zhu, Y.; Mitzi, D. B. *Adv. Energy Mater.* **2014**, *4*, 1301465.

(2) Shin, D.; Saparov, B.; Zhu, T.; Huhn, W. P.; Blum, V.; Mitzi, D. B. *Chem. Mater.* **2016**, *28*, 4771.

(3) Chen, S.; Walsh, A.; Gong, X.-G.; Wei, S.-H. *Adv. Mater.* **2013**, *25*, 1522.

(4) Polizzotti, A.; Repins, I. L.; Noufi, R.; Wei, S.-H.; Mitzi, D. B. *Energy Environ. Sci.* **2013**, *6*, 3171.

(5) Yang, W.; Duan, H.-S.; Cha, K. C.; Hsu, C.-J.; Hsu, W.-C.; Zhou, H.; Bob, B.; Yang, Y. *J. Am. Chem. Soc.* **2013**, *135*, 6915.

(6) Chen, S.; Yang, J.-H.; Gong, X. G.; Walsh, A.; Wei, S.-H. *Phys. Rev. B: Condens. Matter Mater. Phys.* **2010**, *81*, 245204.

(7) Zhou, Y.; Wang, L.; Chen, S.; Qin, S.; Liu, X.; Chen, J.; Xue, D.-J.; Luo, M.; Cao, Y.; Cheng, Y.; Sargent, E. H.; Tang, J. *Nat. Photonics* **2015**, *9*, 409.

(8) Sinsermsuksakul, P.; Sun, L.; Lee, S. W.; Park, H. H.; Kim, S. B.; Yang, C.; Gordon, R. G. *Adv. Energy Mater.* **2014**, *4*, 1400496.

(9) Vaughn, D. D., II; Patel, R. J.; Hickner, M. A.; Schaak, R. E. *J. Am. Chem. Soc.* **2010**, *132*, 15170.

(10) Xue, D.-J.; Tan, J.; Hu, J.-S.; Hu, W.; Guo, Y.-G.; Wan, L.-J. *Adv. Mater.* **2012**, *24*, 4528.

(11) Vaughn, D.; Sun, D.; Levin, S. M.; Biacchi, A. J.; Mayer, T. S.; Schaak, R. E. *Chem. Mater.* **2012**, *24*, 3643.

(12) Antunez, P. D.; Buckley, J. J.; Brutchey, R. L. *Nanoscale* **2011**, *3*, 2399.

(13) Shockley, W.; Queisser, H. J. *J. Appl. Phys.* **1961**, *32*, 510.

(14) Shi, G.; Kioupakis, E. *Nano Lett.* **2015**, *15*, 6926.

(15) Kannewurf, C. R.; Cashman, R. J. *J. Phys. Chem. Solids* **1961**, *22*, 293.

(16) Solanki, G. K.; Deshpande, M. P.; Agarwal, M. K.; Patel, P. D.; Vaidya, S. N. *J. Mater. Sci. Lett.* **2003**, *22*, 985.

(17) Mukherjee, B.; Cai, Y.; Tan, H. R.; Feng, Y. P.; Tok, E. S.; Sow, C. H. *ACS Appl. Mater. Interfaces* **2013**, *5*, 9594.

(18) Yoon, S. M.; Song, H. J.; Choi, H. C. *Adv. Mater.* **2010**, *22*, 2164.

(19) Onodera, A.; Sakamoto, I.; Fujii, Y.; Moλri, N.; Sugai, S. *Phys. Rev. B: Condens. Matter Mater. Phys.* **1997**, *56*, 7935.

(20) Xue, D.-J.; Yang, B.; Yuan, Z.-K.; Wang, G.; Liu, X.; Zhou, Y.; Hu, L.; Pan, D.; Chen, S.; Tang, J. *Adv. Energy Mater.* **2015**, *5*, 1501203.

(21) Sinsermsuksakul, P.; Heo, J.; Noh, W.; Hock, A. S.; Gordon, R. G. *Adv. Energy Mater.* **2011**, *1*, 1116.

(22) Irene, E. A.; Wiedemeier, H. *Z. Anorg. Allg. Chem.* **1975**, *411*, 182.

(23) Ipser, H.; Gambino, M.; Schuster, W. *Monatsh. Chem.* **1982**, *113*, 389.

(24) Major, J. D.; Treharne, R. E.; Phillips, L. J.; Durose, K. *Nature* **2014**, *511*, 334.

(25) Williams, B. L.; Taylor, A. A.; Mendis, B. G.; Phillips, L.; Bowen, L.; Major, J. D.; Durose, K. *Appl. Phys. Lett.* **2014**, *104*, 053907.

(26) Liu, X. H.; Huang, S.; Picraux, S. T.; Li, J.; Zhu, T.; Huang, J. Y. *Nano Lett.* **2011**, *11*, 3991.

(27) Ahn, H.-W.; Seok Jeong, D.; Cheong, B.-k.; Lee, H.; Lee, H.; Kim, S.-d.; Shin, S.-Y.; Kim, D.; Lee, S. *Appl. Phys. Lett.* **2013**, *103*, 042908.

(28) Bosse, J. L.; Grishin, I.; Gyu Choi, Y.; Cheong, B.-k.; Lee, S.; Kolosov, O. V.; Huey, B. D. *Appl. Phys. Lett.* **2014**, *104*, 053109.

(29) Liu, X.; Chen, C.; Wang, L.; Zhong, J.; Luo, M.; Chen, J.; Xue, D.-J.; Li, D.; Zhou, Y.; Tang, J. *Prog. Photovoltaics* **2015**, *23*, 1828.

(30) Kresse, G.; Furthmüller, J. *Phys. Rev. B: Condens. Matter Mater. Phys.* **1996**, *54*, 11169.

(31) Yan, X.; Bain, R. M.; Cooks, R. G. *Angew. Chem., Int. Ed.* **2016**, *55*, 12960.

(32) Wiedemeier, H.; Irene, E. A. *Z. Anorg. Allg. Chem.* **1974**, *404*, 299.

(33) Alaf, M.; Guler, M. O.; Gultekin, D.; Uysal, M.; Alp, A.; Akbulut, H. *Vacuum* **2008**, *83*, 292.

(34) Chandrasekhar, H. R.; Zwick, U. *Solid State Commun.* **1976**, *18*, 1509.

(35) Myung, Y.; Im, H. S.; Kim, C. H.; Jung, C. S.; Cho, Y. J.; Jang, D. M.; Kim, H. S.; Back, S. H.; Park, J. *Chem. Commun.* **2013**, *49*, 187.

(36) Chirilă, A.; Buecheler, S.; Pianezzi, F.; Bloesch, P.; Gretener, C.; Uhl, A. R.; Fella, C.; Kranz, L.; Perrenoud, J.; Seyrling, S.; Verma, R.; Nishiwaki, S.; Romanyuk, Y. E.; Bilger, G.; Tiwari, A. N. *Nat. Mater.* **2011**, *10*, 857.
(37) Guo, Q.; Ford, G. M.; Yang, W.-C.; Walker, B. C.; Stach, E. A.; Hillhouse, H. W.; Agrawal, R. *J. Am. Chem. Soc.* **2010**, *132*, 17384.
(38) De Wolf, S.; Holovsky, J.; Moon, S.-J.; Löper, P.; Niesen, B.; Ledinsky, M.; Haug, F.-J.; Yum, J.-H.; Ballif, C. *J. Phys. Chem. Lett.* **2014**, *5*, 1035.
(39) Chen, C.; Li, W.; Zhou, Y.; Chen, C.; Luo, M.; Liu, X.; Zeng, K.; Yang, B.; Zhang, C.; Han, J.; Tang, J. *Appl. Phys. Lett.* **2015**, *107*, 043905.
(40) Zhou, Y.; Leng, M.; Xia, Z.; Zhong, J.; Song, H.; Liu, X.; Yang, B.; Zhang, J.; Chen, J.; Zhou, K.; Han, J.; Cheng, Y.; Tang, J. *Adv. Energy Mater.* **2014**, *4*, 1301846.
(41) Park, H. H.; Heasley, R.; Sun, L.; Steinmann, V.; Jaramillo, R.; Hartman, K.; Chakraborty, R.; Sinsermsuksakul, P.; Chua, D.; Buonassisi, T.; Gordon, R. G. *Prog. Photovoltaics* **2015**, *23*, 901.
(42) Liu, X.; Chen, J.; Luo, M.; Leng, M.; Xia, Z.; Zhou, Y.; Qin, S.; Xue, D.-J.; Lv, L.; Huang, H.; Niu, D.; Tang, J. *ACS Appl. Mater. Interfaces* **2014**, *6*, 10687.
(43) Speight, J. G. A. *Lange's Handbook of Chemistry*; McGraw Hill Book Co.: New York, 2005.
(44) Frost, J. M.; Walsh, A. *Acc. Chem. Res.* **2016**, *49*, 528.
(45) Shao, Y.; Fang, Y.; Li, T.; Wang, Q.; Dong, Q.; Deng, Y.; Yuan, Y.; Wei, H.; Wang, M.; Gruverman, A.; Shield, J.; Huang, J. *Energy Environ. Sci.* **2016**, *9*, 1752.

DOI: 10.1021/jacs.6b11705
J. Am. Chem. Soc. 2017, 139, 958–965